(E)-4-Methyl-1-tributylstannyl-oct-1-en-6-yn-3-ol: Circular Dichroism Measurement and Determination of the Absolute Configuration by Quantum-chemical CD Calculations

E. N. Voloshina, G. Raabe, J. Fleischhauer, G. J. Kramp, and H.-J. Gais

Institut für Organische Chemie, Rheinisch-Westfälische Technische Hochschule Aachen,
Prof.-Pirlet-Straße 1, 52074 Aachen, Germany.

Reprint requests to J. F.; Fax: +49(0)241/8092385; E-mail: Joerg.Fleischhauer@thc.rwth-aachen.de

The chiroptical properties of the diastereomeric alcohols (E)-(3S,4S)-4-methyl-1-tributylstannyl-oct-1-en-6-yn-3-ol ((S,S)-**3**) and (E)-(3R,4S)-4-methyl-1-tributylstannyl-oct-1-en-6-yn-3-ols ((R,S)-**3**) have been studied experimentally as well as by quantum-chemical calculations. The structures of 20 conformers of each isomer, which were found to represent local minima at the MNDO level, have been optimized with density functional theory (DFT). Based on these geometries the excitation energies and oscillator as well as rotational strengths have been calculated using a time-dependent DFT (TDDFT) method. The CD spectra of the compounds were then obtained as superposition of Boltzmann-weighted spectra for each of the structures. By comparison of the calculated and the experimental CD spectra the absolute configurations have been assigned to the investigated compounds.

Key words: Conformational Analysis; Circular Dichroism; TDDFT Calculations.

1. Introduction

Prostacyclin (**1**) (Fig. 1a), which was discovered by Vane *et al.* [1] in the vascular endothelium, is the most potent endogenous inhibitor of blood platelet aggregation and a strong vasodilator [2, 3]. Unfortunately the medicinal application of **1** is hampered by its short chemical and metabolic half lifes. Intensive synthetic efforts directed towards the discovery of chemically and metabolically more stable and biologically potent analogues of prostacyclin led to the finding of iloprost (**2**, cf. Fig. 1a) by a research team of the Schering AG [4]. Iloprost shows a similar biological profile as the natural compound and exhibits an enhanced chemical and metabolical stability. Iloprost has already been marketed as Ilomedin$^{®}$ for the treatment of patients with ischemic heart and peripheral vascular diseases [5, 6] and it is currently being studied in clinical trails for the treatment of patients with primary pulmonary hypertension, an increasingly common and fatal disease [7, 8]. Ilomedin$^{®}$ is essentially a 1:1 mixture of (16S)- and (16R)-diastereomers. However, it was found that the (16S)-isomer is approximately 5 times more potent than the (16R)-isomer as an inhibitor of ADP-induced platelet aggregation [3]. We are engaged in a program to develop a more efficient asymmetric synthesis of iloprost by using a new strategy [9] whose key step is the conjugate addition of a organometallic C_{13}-C_{20} ω-side chain building block to a bicyclic C_6-C_{12} azoene building block with the stereoselective formation of the C_{12}-C_{13} bond. This strategy required an asymmetric synthesis of the stannyl alcohol (S,S)-**3** (Fig. 1b) having the (15S,16S)-configuration as the ω-side chain building block. Our synthetic efforts, the results of which will be described elsewhere, led to the attainment of a mixture of the enantiomerically pure diastereomeric alcohols (S,S)-**3** and (R,S)-**3** [10], which could be separated by preparative HPLC. Unfortunately assignment of the configuration of the alcohols **3** at C-15 by NMR spectroscopic and other means proved not to be possible. However, for the further synthetic utilization of the $\bar{\omega}$-side chain building block in the planned asymmetric synthesis of **2** knowledge of the absolute configuration of the two diastereomeric alcohols (S,S)-**3** and (R,S)-**3** was of crucial importance. Therefore, we envisioned a determination of the absolute configurations of the diastereomeric alcohols **3** by measurement of their CD spectra and comparison of the calculated and experimental CD spectra [11].

2. Results and Discussion

The experimental CD spectra of the separated diastereomers [10] are shown in Fig. 2a (sample 1) and
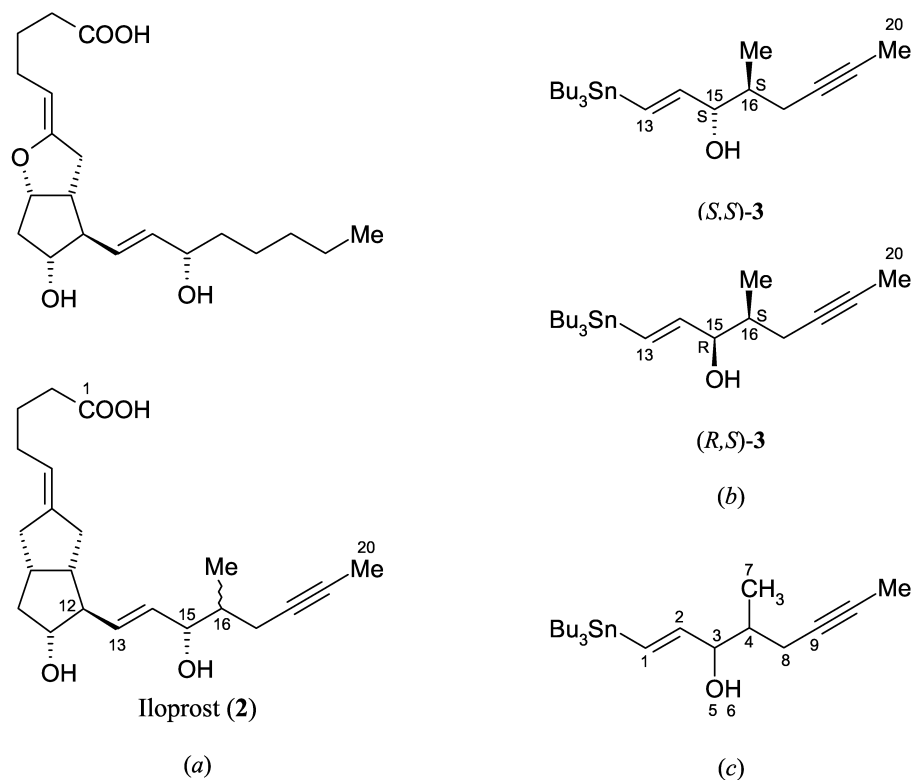
Fig. 1. Structure of prostacyclin (**1**) and iloprost (**2**) (a); diastereomeric side chain building blocks (*S,S*)-**3** and (*R,S*)-**3** (prostaglandine numbering) (b); (E)-4-Methyl-1-tributylstannyl-oct-1-en-6-yn-3-ol (numbering of the atoms used in the discussion) (c).

Fig. 2b (sample 2), respectively. The isomers differ from each other only in the configuration at the chiral centre C^3 (Fig. 1c). The spectrum of sample 1 has its first *Cotton* effect at 235 nm. This band is negative and is relatively weak compared to the second positive one which occurs at 212 nm (Fig. 2a). In the spectrum of sample 2 a strong negative *Cotton* effect observed at about 215 nm corresponds to the positive one in the experimental spectrum of sample 1. In addition a weak shoulder is observed at about 230 nm (Fig. 2b). This shoulder corresponds to the first negative band at $\lambda \approx 235$ nm in the measured spectrum of sample 1.

2.1. Semiempirical Conformational Analysis

Since the two molecules under consideration are very flexible a careful conformational analysis is required to get a reliable CD spectrum. First, a local minimum for each optical isomer has been found with MNDO method [12]. Then the conformer searches have been performed. This search for the (*S,S*)- and the (*R,S*)-isomers of **3** (Fig. 1c) was carried out with the Monte-Carlo method employing the semiempirical MNDO parametrization and the program Spartan [13]. The Monte-Carlo method uses a standard simulated annealing algorithm [14, 15] with a temperature ramp of

$$ T = T_f - \Delta T \left(1 - \frac{I}{I_{max}} \right)^3 , $$

where $\Delta T = T_f - T_i$, T_i and T_f are the initial and final temperatures, respectively; T is the current temperature; I and I_{max} are the current step number and the maximal number of steps, respectively, which depends on the number of the flexible centres of the studied molecule and the number of increments in the rotation. The new conformation is weighted via the Boltzmann criteria ($\exp(\Delta E/kT)$).

The following 4 dihedral angles were chosen to be involved in the search (Fig. 1c): $\angle C^9$-C^8-C^4-C^3, $\angle C^7$-C^4-C^3-C^2, $\angle O^5$-C^3-C^2-C^1, and $\angle H^6$-O^5-C^3-C^2. For
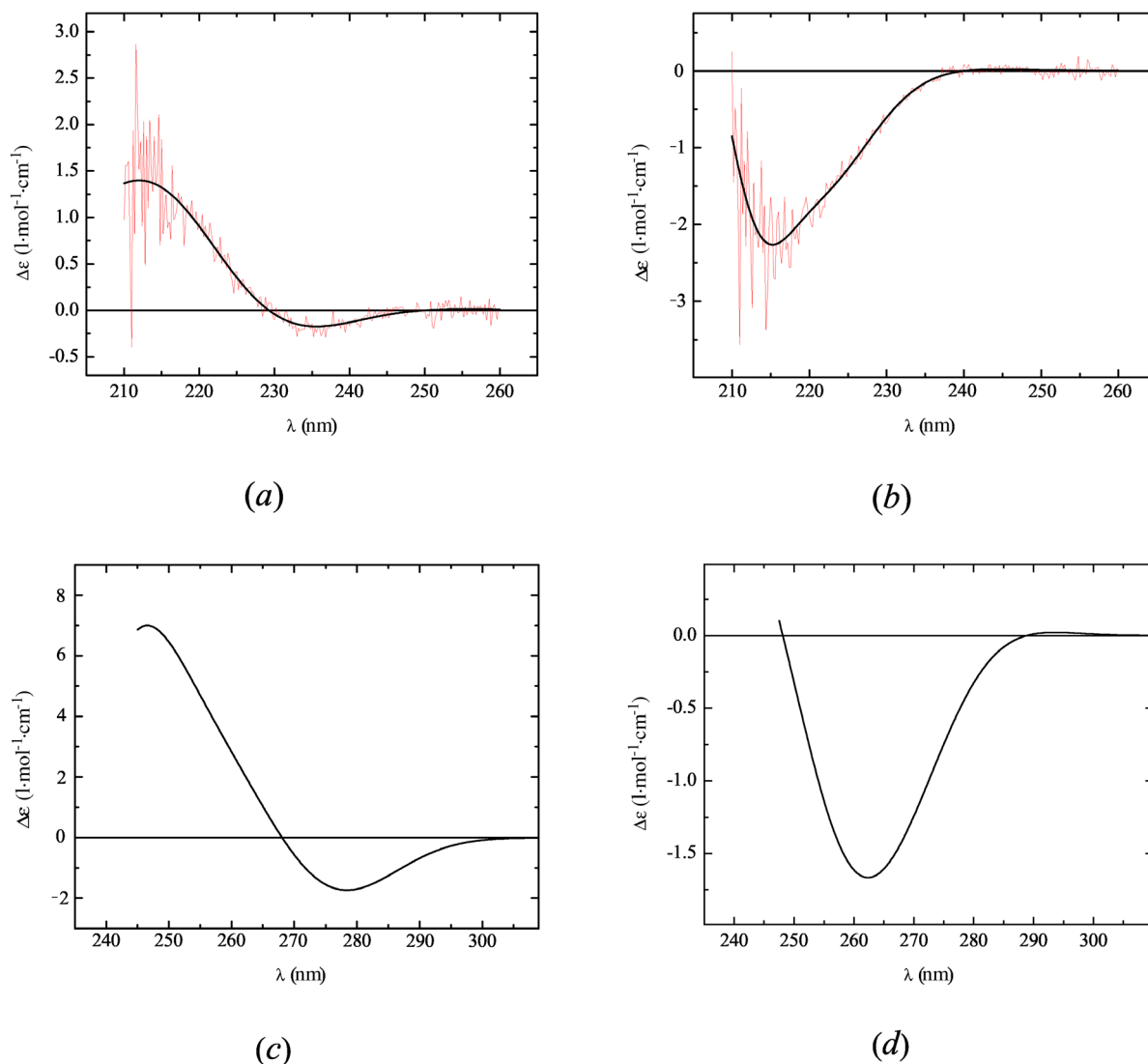
(a)

(b)

(c)

(d)

Fig. 2. Experimental CD spectra of sample 1 (a) and sample 2 (b) (measured in cyclohexane); CD spectra of (*S*,*S*)-**3** (c) and (*R*,*S*)-**3** (d), calculated at TZVP/B-P86 level of TDDFT.

the first three the values 0, 120, and 240 and for the last one the values 0, 90, 180, and 270 were assumed with regard to the initial local minimum.

In our calculations we have used $T_i = 5000$ K, $T_f = 300$ K and $I_{max} = 169$.

The combination of all orientations mentioned above leads to 108 possible conformers for each diastereomer. However, only those conformers whose energies are not more than about 3 kcal/mol above the one of the energetically lowest structure will contribute significantly to the overall CD spectrum. Based on this criterium only the 20 energetically lowest conformers for (*S*,*S*)-**3** and for (*R*,*S*)-**3** have further been considered in the calculation of the chiroptical properties.

2.2. Geometry Optimization with DFT Method

The corresponding 20 conformers obtained at the MNDO level were reoptimized with a density functional theory (DFT) method, as implemented in the *TURBOMOLE* set of programs [16, 17], using the B-P86 functional [18] and a TZVP (Triple-ζ Valence plus

Table 1. DFT-optimized structural parameters and relative energies of the conformers of (S,S)-**3**.

Confor-mer	Geometry				Relative energy (kcal/mol)	w_i[a] %
	$\angle C^9$-C^8 -C^4-C^3	$\angle C^7$-C^4 -C^3-C^2	$\angle O^5$-C^3 -C^2-C^1	$\angle H^6$-O^5 -C^3-C^2		
a	172.106	59.569	113.969	−51.690	0.00	27.6[b]
b	−65.659	60.135	113.969	−52.697	0.06	24.9[b]
c	172.969	171.390	126.667	−53.097	0.78	7.4
d	170.915	167.680	−6.862	−51.684	0.91	5.9
e	171.674	54.099	−15.922	−51.111	1.08	4.5
f	170.803	−58.644	119.069	−49.285	1.11	4.2
g	172.099	54.289	−15.187	51.206	1.16	3.9
h	169.478	168.843	8.869	47.842	1.18	3.8
i	−68.208	50.459	8.419	47.788	1.25	3.3
j	169.187	50.356	8.536	47.810	1.28	3.2
k	169.533	167.817	5.628	−48.135	1.32	3.0
l	168.348	53.054	−2.908	59.799	1.50	2.2
m	174.184	171.296	2.603	−172.053	1.58	1.9
n	167.490	−62.986	−11.960	−47.932	1.90	1.1
o	45.294	−63.043	−11.588	−47.947	1.94	1.0
p	166.308	−61.047	5.920	54.434	2.22	0.6
r	177.758	176.298	142.902	−176.902	2.42	0.5
s	170.545	−59.746	118.374	59.504	2.58	0.4
t	169.622	−57.797	129.213	175.844	2.62	0.3
u	165.640	−61.585	−3.140	−179.596	2.81	0.2

Table 2. DFT-optimized structural parameters and relative energies of the conformers of (R,S)-**3**.

Con-for-mer	Geometry				Relative energy (kcal/mol)	w_i[a] %
	$\angle C^9$-C^8 -C^4-C^3	$\angle C^7$-C^4 -C^3-C^2	$\angle O^5$-C^3 -C^2-C^1	$\angle H^6$-O^5 -C^3-C^2		
a	174.436	176.165	−115.863	51.100	0.00	14.9[b]
b	62.089	67.504	4.007	59.404	0.01	14.6[b]
c	173.026	66.029	−8.659	−54.713	0.12	12.2
d	64.929	69.159	8.648	57.687	0.30	9.0
e	61.813	62.718	−127.888	58.299	0.31	8.8
f	171.527	66.045	7.211	52.061	0.34	8.4
g	−175.527	67.463	4.088	59.970	0.35	8.3
h	169.637	59.775	−125.654	52.557	0.49	6.5
i	169.678	64.903	4.429	52.720	0.50	6.4
j	−65.922	65.167	−144.098	−169.969	0.70	4.6
k	−80.878	−65.621	−118.052	46.886	1.27	1.7
l	174.702	177.862	−112.444	−60.715	1.32	1.6
m	178.415	−177.831	17.663	50.071	1.43	1.3
n	166.801	62.763	−6.536	161.864	1.73	0.8
o	175.529	171.437	−127.802	−179.081	1.92	0.6
p	−80.225	−86.857	163.705	−2.454	2.98	0.09
r	61.384	−81.548	−125.258	46.366	3.35	0.06
s	−75.349	72.012	5.640	55.631	3.51	0.04
t	−74.530	70.503	−121.592	54.576	3.59	0.03
u	77.296	−66.848	9.680	46.661	4.05	0.01

[a] $w_i = \exp(-E_i/RT)/\sum_{j=1}^{N}\exp(-E_j/RT)$ is the Boltzmann factor of the *i*-th local minimum, where E_i is the energy of this local minimum, N is the number of local stationary points. [b] The corresponding 3D structures are given in Figure 3.

Table 3. The electronic configurations, calculated oscillator and rotational strengths for the first 5 excited states of conformers *a-c*, *f* of (S,S)-**3**. θ is the angle between the electric and the magnetic dipole moment[c].

Wave-length (nm)	Trans-ition	Type	Contri-bution (%)	θ (degree)	Oscillator Strength	Rotational Strength (*)
(S,S)-**3a** ($w = 27.6\%$):						
281.2	$89 \rightarrow 90$	$\pi \rightarrow \pi*$	98.2	82.0	0.0001	−0.21
275.7	$88 \rightarrow 90$	$\pi \rightarrow \pi*$	95.6	70.7	0.0374	−8.36
257.9	$87 \rightarrow 90$	$\sigma,\pi \rightarrow \pi*$	55.7	74.6	0.0341	10.44
	$86 \rightarrow 90$	$\sigma \rightarrow \pi*$	31.0			
254.3	$86 \rightarrow 90$	$\sigma \rightarrow \pi*$	67.9	90.4	0.0475	3.98
	$87 \rightarrow 90$	$\sigma,\pi \rightarrow \pi*$	24.2			
244.0	$85 \rightarrow 90$	$\sigma,n \rightarrow \pi*$	87.2	125.9	0.0212	21.45
(S,S)-**3b** ($w = 24.9\%$):						
282.5	$89 \rightarrow 90$	$\pi \rightarrow \pi*$	98.2	79.8	0.0001	−0.53
276.9	$88 \rightarrow 90$	$\pi \rightarrow \pi*$	94.2	98.5	0.0347	−8.03
259.1	$87 \rightarrow 90$	$\sigma,\pi \rightarrow \pi*$	82.1	88.1	0.0652	0.65
257.3	$86 \rightarrow 90$	$\sigma \rightarrow \pi*$	93.9	78.1	0.0068	1.55
244.3	$85 \rightarrow 90$	$\sigma,n \rightarrow \pi*$	90.4	63.5	0.0131	13.47

Table 3 (continued).

Wave-length (nm)	Trans-ition	Type	Contri-bution (%)	θ (degree)	Oscillator Strength	Rotational Strength (*)
(S,S)-**3c** ($w = 7.4\%$):						
278.3	$89 \rightarrow 90$	$\pi \rightarrow \pi*$	66.3	149.5	0.0010	−2.08
	$88 \rightarrow 90$	$\pi \rightarrow \pi*$	32.4			
275.9	$88 \rightarrow 90$	$\pi \rightarrow \pi*$	63.5	63.5	0.0204	10.85
	$89 \rightarrow 90$	$\pi \rightarrow \pi*$	26.6			
257.1	$87 \rightarrow 90$	$\sigma,\pi \rightarrow \pi*$	80.3	84.4	0.0760	7.54
254.7	$86 \rightarrow 90$	$\sigma \rightarrow \pi*$	94.0	93.8	0.0047	−0.35
246.2	$85 \rightarrow 90$	$\sigma,n \rightarrow \pi*$	90.6	88.5	0.0042	−1.32
(S,S)-**3f** ($w = 4.2\%$):						
278.0	$89 \rightarrow 90$	$\pi \rightarrow \pi*$	66.5	77.9	0.0062	1.97
	$88 \rightarrow 90$	$\pi \rightarrow \pi*$	32.7			
274.9	$88 \rightarrow 90$	$\pi \rightarrow \pi*$	48.8	91.3	0.0076	−0.27
	$87 \rightarrow 90$	$\pi \rightarrow \pi*$	30.8			
261.6	$87 \rightarrow 90$	$\pi \rightarrow \pi*$	53.4			
	$88 \rightarrow 90$	$\pi \rightarrow \pi*$	12.3	61.6	0.0409	10.93
	$85 \rightarrow 90$	$\sigma,n \rightarrow \pi*$	10.6			
258.9	$86 \rightarrow 90$	$\sigma \rightarrow \pi*$	83.0	90.1	0.0202	−1.42
249.4	$85 \rightarrow 90$	$\sigma,n \rightarrow \pi*$	84.4	54.8	0.0133	18.25

[c] In cases where this angle is close to 90° the sign of the corresponding *Cotton* effect is very sensitive even to small changes of the molecular structure. (*) $\times 10^{-40}$erg·cm³.

Polarization) [19] basis set. For the Sn atom an effective core potential (ECP) has been used. In these calculations, the default ECP parameters supplied by *TURBOMOLE* [16] were adopted. Some selected dihedral angles of the resulting structures and their rel-

ative energies are given in Tables 1 and 2 for (S,S)-**3** and (R,S)-**3**, respectively. Optimized 3D structures of

(S,S)-**3a**
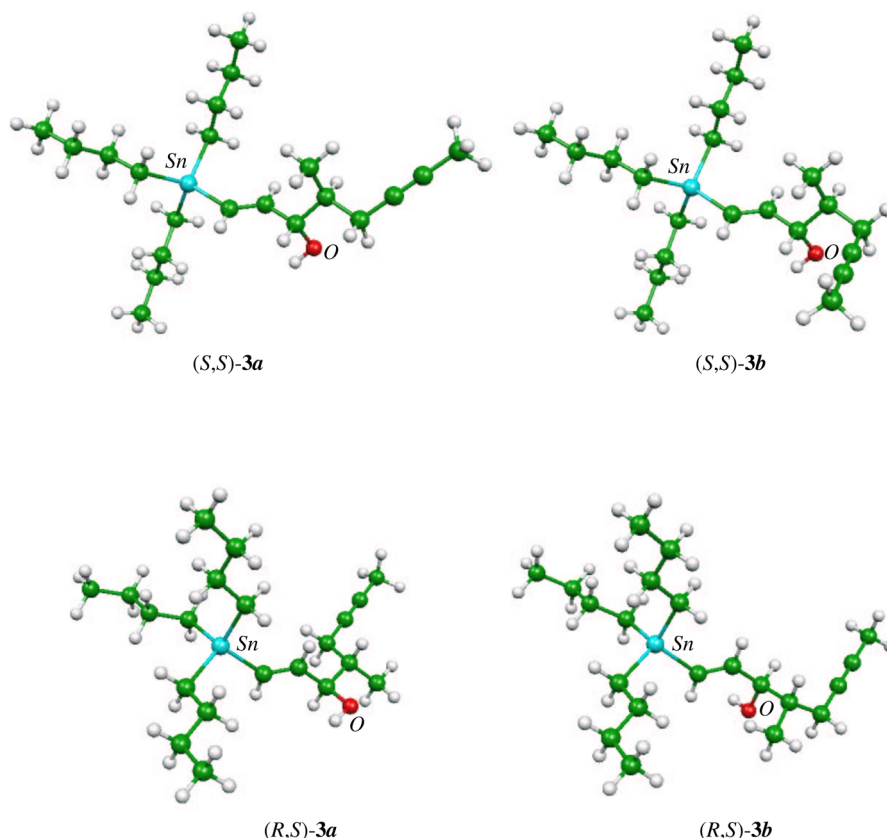
(S,S)-**3b**

(R,S)-**3a**

(R,S)-**3b**

Fig. 3. 3D structures of the most stable conformers of (S,S)-**3** and (R,S)-**3** calculated at TZVP/B-P86 level of DFT.

the most stable conformers (S,S)-**3a**, (S,S)-**3b**, (R,S)-**3a**, and (R,S)-**3b** are shown in Figure 3.

Since the experimental spectra were measured in cyclohexane, we assumed that due to the low dielectric constant of the solvent ($\varepsilon = 2.0$) it is not necessary to reoptimize the obtained geometries under the influence of the solvent (for example, by an electrostatic continuum model (COSMO, conductor-like screen model [16])).
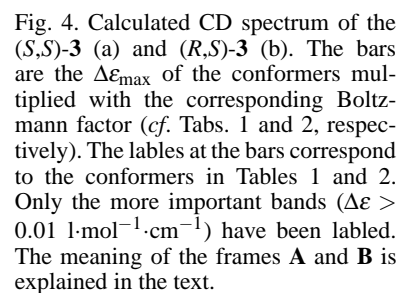
2.3. TDDFT Calculations

The excitation energies and rotational strengths of the 25 lowest-lying singlet excited states were calculated using the time-dependent DFT (TDDFT) [20] method with the same functional and basis set as mentioned above. For the calculation of the rotational strengths the origin-independent dipole velocity approximation has been used [21].

The CD curves have been calculated as a sum of Gaussians, each of which is centered at the calculated wavelength of the corresponding transition and mul-

tiplied with its rotational strength [22]. The Gaussians were generated using the empirical formula $\Gamma = k \cdot \lambda^{1.5}$ for the half bandwidth Γ at ε_{max}/e [23]. The parameter k was set to $2.887 \cdot 10^{-3}$, which yields a half bandwidth $\Gamma \approx 10$ nm for an absorption band at $\lambda \approx 220$ nm. The individually calculated CD spectra for the energetically lowest 20 conformers of (S,S)-**3** and (R,S)-**3** were Boltzmann-weighted (Boltzmann factors are given in Tables 1 and 2, respectively) and added up to give the computed overall CD spectra for the (S,S)- and (R,S)-isomers of **3** given in Figs. 2c and 2d, respectively. Compared with the experimental spectra the calculated ones are shifted by about 45 nm to the red.

Our TDDFT calculations predict these 25 transitions to occur in the range between 190 – 285 nm in the CD spectra of the conformers of (S,S)-**3** and (R,S)-**3**. The first 5 rotational strengths of all conformers of (S,S)-**3** and (R,S)-**3** each of which is multiplied with its Boltzmann factor are displayed in Figs. 4a and 4b, respectively. It can be clearly seen that in the case of (S,S)-**3** only conformers ***a-c*** and ***f*** contribute significantly to the calculated average CD spectrum (Fig. 4a),

Fig. 4. Calculated CD spectrum of the (S,S)-**3** (a) and (R,S)-**3** (b). The bars are the $\Delta\varepsilon_{max}$ of the conformers multiplied with the corresponding Boltzmann factor (*cf.* Tabs. 1 and 2, respectively). The lables at the bars correspond to the conformers in Tables 1 and 2. Only the more important bands ($\Delta\varepsilon >$ 0.01 $l \cdot mol^{-1} \cdot cm^{-1}$) have been labled. The meaning of the frames **A** and **B** is explained in the text.

whereas in the case of (R,S)-**3** the first 10 conformers dominate the CD spectrum (Fig. 4b). The relevant configurations for the first 5 states of conformers are listed in Tables 3 and 4, respectively, together with the calculated oscillator and rotational strengths. In addition we also list the angles θ between the electric and the magnetic transition dipole moments. The Kohn-Sham orbitals (KSOs) $\Psi_{85} - \Psi_{90}$ of the most stable conformers of (S,S)-**3** and (R,S)-**3** are displayed in Figs. 5 and 6, respectively. From these figures it can be seen that Sn does not contribute significantly to these KSOs.

Table 4. The electronic configurations, calculated oscillator and rotational strengths for the first 5 excited states of the conformers *a-j* of the (R,S)-**3**. θ is the angle between the electric and the magnetic dipole moment.

Table 4 (continued).

Wave-length (nm)	Trans-ition	Type	Contri-bution (%)	θ (degree)	Oscillator Strength	Rotational Strength (*)
(R,S)-**3a** (w = 14.9%):						
273.3	89 → 90	$\pi \to \pi*$	64.4	107.4	0.0069	−2.62
	88 → 90	$\pi \to \pi*$	33.5			
270.4	88 → 90	$\pi \to \pi*$	55.9	143.7	0.0052	−1.58
	87 → 90	$\sigma,\pi \to \pi*$	21.9			
254.7	86 → 90	$\sigma \to \pi*$	85.8	115.8	0.0057	−1.21
254.0	87 → 90	$\sigma,\pi \to \pi*$	65.7	88.4	0.1087	1.04
	89 → 90	$\pi \to \pi*$	9.6			
245.6	85 → 90	$\sigma,n \to \pi*$	85.8	85.1	0.0035	2.78
(R,S)-**3b** (w = 14.7%):						
255.5	88 → 90	$\pi \to \pi*$	53.9	78.31	0.0367	3.73
	89 → 90	$\pi \to \pi*$	41.5			
251.1	88 → 90	$\pi \to \pi*$	40.5	96.36	0.1159	−10.26
	89 → 90	$\pi \to \pi*$	33.6			
243.7	86 → 90	$\sigma,\pi \to \pi*$	82.0	126.45	0.0039	−3.31
242.7	87 → 90	$\sigma,\pi \to \pi*$	60.2	84.98	0.0378	2.33
	89 → 90	$\pi \to \pi*$	12.4			
233.1	85 → 90	$\sigma,n \to \pi*$	94.1	90.11	0.0035	0.52
(R,S)-**3c** (w = 12.2%)						
259.5	88 → 90	$\pi \to \pi*$	63.8	62.8	0.0337	−6.43
	89 → 90	$\pi \to \pi*$	16.4			
255.1	87 → 90	$\pi \to \pi*$	49.4	91.2	0.0897	−11.18
	89 → 90	$\pi \to \pi*$	32.3			
248.3	86 → 90	$\sigma \to \pi*$	44.3	118.1	0.0162	6.10
	87 → 90	$\pi \to \pi*$	26.9			
246.6	86 → 90	$\sigma \to \pi*$	55.2	52.4	0.0081	5.03
	87 → 90	$\pi \to \pi*$	21.8			
235.8	85 → 90	$\sigma,n \to \pi*$	89.1	70.9	0.0511	−11.94
264.7	89 → 90	$\pi \to \pi*$	57.5	96.6	0.0153	−3.05
	88 → 90	$\pi \to \pi*$	41.5			
259.7	88 → 90	$\pi \to \pi*$	38.5	99.3	0.0635	−15.88
	87 → 90	$\pi \to \pi*$	36.6			
250.1	87 → 90	$\pi \to \pi*$	58.8	44.9	0.0550	16.53
	88 → 90	$\pi \to \pi*$	16.5			
249.2	86 → 90	$\sigma \to \pi*$	99.5	124.3	0.0021	−1.00
232.8	85 → 90	$\sigma,n \to \pi*$	92.2	112.0	0.0086	−15.14
(R,S)-**3e** (w = 8.8%):						
259.6	89 → 90	$\pi \to \pi*$	50.2	79.8	0.0373	5.12
	88 → 90	$\pi \to \pi*$	44.0			
254.5	88 → 90	$\pi \to \pi*$	49.7	96.8	0.0960	−10.49
	89 → 90	$\pi \to \pi*$	25.6			
247.3	86 → 90	$\sigma \to \pi*$	63.9	63.2	0.0095	6.85
	87 → 90	$\pi \to \pi*$	29.3			
245.2	87 → 90	$\pi \to \pi*$	45.1	81.2	0.0276	4.53
	86 → 90	$\sigma \to \pi*$	34.9			
235.1	85 → 90	$\sigma,n \to \pi*$	95.5	108.4	0.0035	−4.21
(R,S)-**3f** (w = 8.4%):						
272.7	89 → 90	$\pi \to \pi*$	52.6	115.8	0.0138	−5.99
	88 → 90	$\pi \to \pi*$	40.1			
268.6	88 → 90	$\pi \to \pi*$	53.1	95.1	0.0324	−3.13
	87 → 90	$\pi \to \pi*$	23.6			
257.8	87 → 90	$\pi \to \pi*$	51.3	89.1	0.0293	0.13
	86 → 90	$\sigma \to \pi*$	22.7			
254.2	86 → 90	$\sigma \to \pi*$	73.3	80.5	0.0336	3.64
247.8	85 → 90	$\sigma,n \to \pi*$	92.6	108.9	0.0033	−5.05
(R,S)-**3g** (w = 8.3%):						
280.3	89 → 90	$\pi \to \pi*$	96.4	62.5	0.0010	2.04
275.4	88 → 90	$\pi \to \pi*$	85.2	85.1	0.0306	5.75
260.0	87 → 90	$\sigma,\pi \to \pi*$	63.8	83.7	0.0512	3.97
	86 → 90	$\sigma \to \pi*$	19.8			
256.5	86 → 90	$\sigma \to \pi*$	79.5	89.8	0.0301	1.66
246.6	85 → 90	$\sigma,n \to \pi*$	93.8	116.3	0.0126	−11.02
(R,S)-**3h** (w = 6.5%):						
267.9	89 → 90	$\pi \to \pi*$	72.0	76.1	0.0004	0.56
263.3	88 → 90	$\pi \to \pi*$	49.1	94.7	0.0648	−10.54
	87 → 90	$\pi \to \pi*$	26.7			
250.6	87 → 90	$\pi \to \pi*$	56.2	20.1	0.0521	16.00
	86 → 90	$\sigma \to \pi*$	15.1			
250.4	86 → 90	$\sigma \to \pi*$	84.1	68.2	0.0168	3.44
236.1	85 → 90	$\sigma,n \to \pi*$	90.5	54.2	0.0233	15.22
(R,S)-**3i** (w = 6.4%):						
257.6	89 → 90	$\pi \to \pi*$	80.8	67.1	0.0795	13.11
250.7	87 → 90	$\pi \to \pi*$	98.6	107.4	0.0043	−1.04
250.1	88 → 90	$\pi \to \pi*$	88.7	85.5	0.0198	1.41
241.5	86 → 90	$\sigma \to \pi*$	92.7	31.6	0.0018	7.97
237.8	85 → 90	$\sigma,n \to \pi*$	96.6	19.6	0.0011	4.22
(R,S)-**3j** (w = 4.6%):						
266.1	88 → 90	$\pi \to \pi*$	94.3	69.3	0.0013	1.17
264.9	89 → 90	$\pi \to \pi*$	48.9	108.3	0.0120	−3.82
	87 → 90	$\pi \to \pi*$	47.8			
252.9	87 → 90	$\pi \to \pi*$	42.4	99.5	0.0813	−8.87
	89 → 90	$\pi \to \pi*$	33.3			
252.1	85 → 90	$\sigma,n \to \pi*$	88.5	94.1	0.0173	−1.12
248.4	86 → 90	$\sigma \to \pi*$	92.3	44.8	0.0009	8.12

(*) $\times 10^{-40}$ erg·cm^3.

According to the TDDFT results the first *Cotton* effect in the average CD spectrum of (S,S)-**3** is negative and due to $\pi \to \pi*$ transitions from three upper MOs (Ψ_{89} (HOMO), Ψ_{88}, Ψ_{87}) to the LUMO (Ψ_{90}) (Fig. 4a, Frame **A**). The next *Cotton* effect is predicted to be positive. It is the resultant of several transitions, and $\sigma \to \pi*$ transitions to the LUMO ($\Psi_{86} \to \Psi_{90}$, $\Psi_{85} \to \Psi_{90}$) (Fig. 4a, Frame **B**) give the main contributions to this band (Tab. 3, Fig. 5).

As can be expected the theoretical CD spectrum of the second compound ((R,S)-**3**) spreads over the same

85th KSO, σ+*n*
(-6.31 eV)

86th KSO, σ
(-6.22 eV)

87th KSO, σ+π
(-6.00 eV)

88th KSO, π
(-5.86 eV)

89th KSO, π
(-5.79 eV)
(HOMO)

90th KSO, π*
(-1.40 eV)
(LUMO)

Fig. 5. Kohn-Sham orbitals Ψ_{85} to Ψ_{90} of the most stable conformer of (*S,S*)-**3**. Ψ_{89} and ψ_{90} are the HOMO and the LUMO, respectively.

85th KSO, σ+*n*
(-6.25 eV)

86th KSO, σ
(-6.21 eV)

87th KSO, σ+π
(-6.04 eV)

88th KSO, π
(-5.92 eV)

89th KSO, π
(-5.88 eV)
(HOMO)

90th KSO, π*
(-1.37 eV)
(LUMO)

Fig. 6. Kohn-Sham orbitals Ψ_{85} to Ψ_{90} of the most stable conformer of (*R,S*)-**3**. Ψ_{89} and Ψ_{90} are the HOMO and the LUMO, respectively.

spectral region as the first one. A detailed analysis of the individual spectra calculated for the (R,S)-**3** conformers reveals 2 groups of transitions in this spectrum: the first one covers the range between about $\lambda \sim 270 - 280$ nm (Fig. 4b, Frame **A**) and corresponds to the first negative *Cotton* effect in the spectrum of (S,S)-**3**. The other one occurs in the region between 245 and 265 nm (Fig. 4b, Frame **B**) and is, therefore, close to the second *Cotton* effect of the first compound (cf. Fig. 4a, Frame **B**). Since the first and the second groups of transitions occur at similar wavelengths and have mostly rotational strengths of the same sign (negative), they are not clearly resolved but coincide to give one negative *Cotton* effect.

A comparison of the experimental and the calculated CD spectra in Figs. 2a and 2c, 2b and 2d shows that not only the signs of the *Cotton* effects but also the general appearance of the theoretical spectra calculated for (S,S)-**3** and (R,S)-**3** agree with those observed for sample 1 and sample 2. Thus, we conclude, that samples 1 and 2 contain the (S,S)- and the (R,S)-isomer of **3**, respectively.

3. Experimental Part

For the CD measurements samples were dissolved in cyclohexane ($c_{sample1} = 4.704 \cdot 10^{-4}$ mol/l; $c_{sample2} = 5.604 \cdot 10^{-4}$ mol/l). The CD spectra were measured on a Circular Dichroism spectrometer (AVIV Model 62DS) at room temperature.

The thin solid lines through the data points (Fig. 2a,b) have been obtained by a point averaging FFT (Fast Fourier Transformation) smoothening procedure.

[1] S. Moncada, R. J. Gryglewski, S. Bunting, and J. R. Vane, Nature, London **263**, 633 (1976).

[2] P. W. Collins and S. W. Djuric, Chem. Rev. **93**, 1533 (1993).

[3] Prostacyclin and Its Stable Analogue Iloprost; R. J. Gryglewski and G. Stock, Eds. Springer Verlag, Berlin 1987.

[4] W. Skuballa and H. Vorbrüggen. Angew. Chem. 93, 1080 (1981); Angew. Chem. Int. Ed. Engl. **20**, 1046 (1981).

[5] S. Duthois, N. Cailleux, and H. Levesque, J. Malad. Vasc. **25**, 17 (2000).

[6] E. B. Melian and K. L. Goa, Drug **62**, 107 (2002).

[7] E. Spiekerkoetter, H. Fabel, and M. M. Hoeper, Deut. Ärztebl. **98**, A2104 (2001).

[8] H. Olschewski, G. Simonneau, G. Nazzareno, T. Higenbottam, R. Naeije, J. R. Rubin, S. Nikkho, R. Speich, M. M. Hoeper, J. Behr, J. Winkler, O. Sitbon, W. Popov, H. A. Ghofrani, A. Manes, D. G. Kiely, R. Ewert, A. Meyer, P. A. Corris, M. Delcroix, M. Gomez-Sanchez, H. Siedentop, and W. Seegers, N. Engl. J. Med. **347**, 322 (2002).

[9] M. van Bergen and H.-J. Gais, J. Amer. Chem. Soc. **124**, 4321 (2002).

[10] G. J. Kramp and H.-J. Gais, unpublished results.

[11] Y. Wang, G. Raabe, C. Repges, and J. Fleischhauer, Int. J. Quant. Chem. **93**, 265 (2003).

[12] M. J. S. Dewar and W. Thiel. J. Amer. Chem. Soc. **99**, 1285 (1977).

[13] Spartan (Version 5.0), Wavefunction, Inc. 18401 Von Karman Ave., Suite 370, Irvine, CA 92612, USA.

[14] http://pages.pomona.edu/∼wsteinmetz/chem164/ confsearch_spartan.doc; http://www.ugcs.caltech.edu/ info/gsl/siman_1.html.

[15] N. Metropolis, A. W. Rosenbluth, M. N. Rosenbluth, A. H. Teller, and E. Teller, J. Chem. Phys. **21**, 1087 (1953).

[16] TURBOMOLE (Version 4), R. Ahlrichs, M. Bär, H.-P. Baron, R. Bauernschmitt, S. Böcker, M. Ehrig, K. Eichkorn, S. Elliott, F. Furche, F. Haase, M. Häser, H. Horn, C. Huber, U. Huniar, M. Kattannek, C. Kölmel, M. Kollwitz, K. May, C. Ochsenfeld, H. Öhm, A. Schäfer, U. Schneider, O. Treutler, M. von Arnim, F. Weigend, P. Weis, and H. Weis, Quantum Chemistry Group, University of Karlsruhe, Germany 1999.

[17] R. Ahlrichs, In: Encyclopedia of Computational Chemistry. P. v. R. Schleyer, (Ed.) TURBOMOLE. Wiley, Chichester 1998; Vol. 5, pp. 3123 – 3129.

[18] A. D. Becke, Phys. Rev. A. **5**, 3098 (1988); J. P. Perdew, Phys. Rev. B. **33**, 8822 (1986).

[19] A. Schäfer, C. Huber, and R. Ahlrichs, J. Chem. Phys. **100**, 5829 (1994).

[20] F. Furche, R. Ahlrichs, C. Wachsmann, E. Weber, A. Sobanski, F. Vögtle, and S. Grimme, J. Amer. Chem. Soc. **122**, 1717 (2000).

[21] A. Moscowitz, in O. Sinanoglu (ed.), Modern Quantum Chemistry, John Wiley & Sons, Inc., New York 1965, Vol.3, P21.

[22] J. A. Schellman, Chem. Rev. **75**, 323 (1975).

[23] G. Kurapkat, P. Krüger, A. Wollmer, J. Fleischhauer, B. Kramer, E. Zobel, A. Koslowski, H. Botterweck, and R. W. Woody, Biopolymers. **41**, 267 (1997).